Advanced Laser Development and Plasma-Physics Studies on the Multi-Terawatt Laser

I. A. Begishev,[1] V. Bagnoud,[2] S.-W. Bahk,[1] W. A. Bittle,[1] G. Brent,[1] R. Cuffney,[1] C. Dorrer,[1] D. H. Froula,[1] D. Haberberger,[1] C. Mileham,[1] P. M. Nilson,[1] A. V. Okishev,[1,†] J. L. Shaw,[1] M. J. Shoup III,[1] C. R. Stillman,[1,3] C. Stoeckl,[1] D. Turnbull,[1] B. Wager,[1] J. D. Zuegel,[1] and J. Bromage[1]

[1]Laboratory for Laser Energetics, University of Rochester
[2]GSI - Helmholtzzentrum für Schwerionenforschung GmbH, Germany
[3]Image Science, Space and Airborne System, L3Harris Technologies
[†]Deceased

The Multi-Terawatt (MTW) laser, built initially as the prototype front end for a petawatt laser system, is a 1053-nm hybrid system with gain from optical parametric chirped-pulse amplification (OPCPA) and Nd:glass. Compressors and target chambers were added, making MTW a complete laser facility (output energy up to 120 J, pulse duration from 20 fs to 2.8 ns) for studying high-energy-density physics and developing short-pulse laser technologies and target diagnostics. Further extensions of the laser support the ultrahigh-intensity laser development of an all-OPCPA system and a Raman plasma amplifier.

Fundamental research in high-energy-density physics[1] and materials science[2] has accelerated the development of kilojoule and megajoule lasers;[3–9] however, the deployment of these lasers is limited because of the cost and complexity of construction and operation. The low repetition rates (typically a few shots per day) hinders the mapping of large parameter spaces and statistical averaging. Midscale lasers producing hundreds of joules with subpetawatt peak power provide more flexibility and user access at higher repetition rates. Lasers at this scale enable technologies to be developed and tested before they are implemented on large-scale facilities. They also serve as experimental platforms for scientific research in their own right.

This summary describes LLE's MTW laser, a midscale laser system built initially as the prototype front end for OMEGA EP.[4] Currently, MTW operates at 1053 nm, where gain is provided by a combination of optical parametric amplification in nonlinear crystals and laser amplification in neodymium-doped glass. A pulse compressor and three target chambers have been added, making MTW a complete facility for plasma-physics research and laser science, as well as a development platform for laser technologies, large-area damage tests, and target diagnostics. MTW is also open for external users to conduct experiments.

Separate broadband and narrowband front ends produce synchronized nanosecond pulses for the OPCPA seed and pump, respectively. The narrowband pulse is amplified in three Nd:YLF amplifiers and frequency doubled before it pumps the OPCPA crystals. The resulting broadband signal pulse is further amplified in two Nd:glass amplifiers. After the picosecond compressor, pulses can be directed to the spherical target chamber (STC), the cylindrical target chamber (CTC), or the underdense plasma (UDP) chamber. As an option, the picosecond compressor can be bypassed to allow nanosecond pulses to propagate directly to each target chamber.

MTW can also be configured in a narrowband mode. In this case, the output of the Nd:YLF amplifiers goes directly to the Nd:glass amplifiers. This mode is mainly used to pump the final stage of an ultra-broadband optical parametric amplifier line (OPAL) after second-harmonic generation. It supports the generation of >10-J, >140-nm pulses,[10] which are compressed in the femtosecond compressor and delivered to the UDP chamber. Table I summarizes the range of parameters and applications of the broadband and narrowband modes of operation for the MTW Laser System. A general view of the MTW Laser System from the end of the system shows the picosecond grating compressor chamber (ps-GCC), the STC, and the CTC (Fig. 1).

Table I: Parameters and main applications of the MTW laser.

| Mode	Application	λ (nm)	E (J)	τ (ps)
Broadband	Large-area damage tests	1053	120	2400
	High-energy-density physics, x-ray and neutron diagnostics	1053, 527	35 to 50	0.5 to 100
	Raman plasma amplification	1053, 527	35 to 40	0.5 to 100
	Ultrafast streak-camera development	1053, 264	0.1 (5 Hz)	0.5 to 100
Narrowband	Pump for all OPCPA lasers	527	50	1600
	5ω generation development	527, 263, 211	1.2 (5 Hz)	1000 to 2800
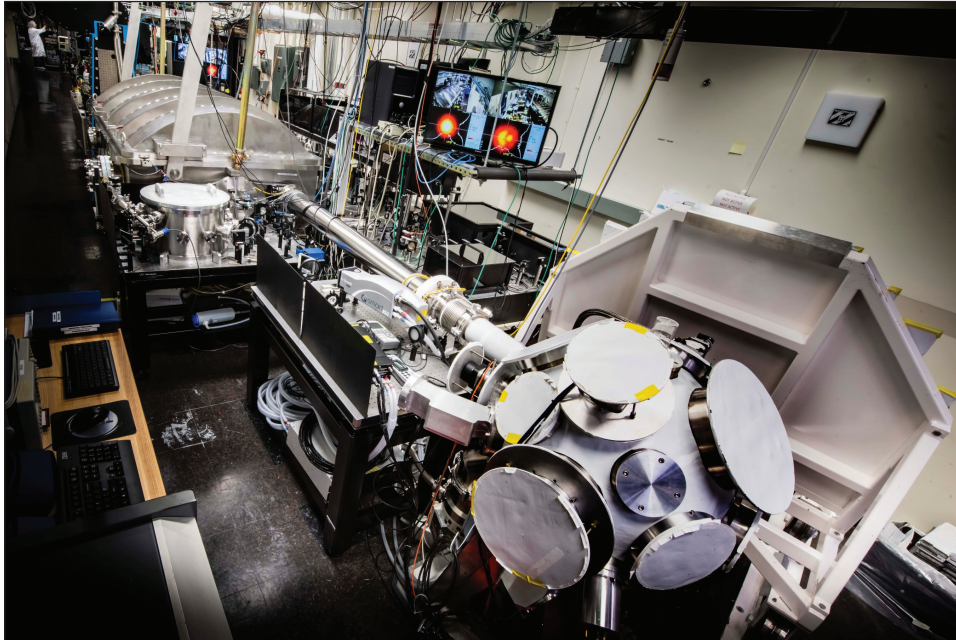
Figure 1
General view of the MTW Laser System from the spherical target chamber side.

G13292JR

A detailed layout of the MTW laser is shown in Fig. 2. Depending on the desired operation mode, switchyards (SY's) 1 to 5 (indicated as blue circles) using mirrors on kinematic or translation stages send beams along different paths. The broadband front end consists of a commercial femtosecond master oscillator, an ultrafast optical parametric amplifier (UOPA) for increased temporal contrast, and a pulse stretcher. The narrowband front end includes a pulse-shaping system,[11] a diode-pumped regenerative amplifier (regen),[12] and a crystal large-aperture ring amplifier (CLARA),[13] all operating at 1053 nm. The amplified narrowband beam is frequency converted to the second harmonic to pump the OPCPA stages,[14] which are seeded by the broadband front end. The UOPA provides approximately four-orders-of-magnitude energy amplification while restricting the associated parametric fluorescence to a few picoseconds around the output pulse.[15] This makes it possible to reduce the required gain in the OPCPA stages, where the pump pulse has a duration of a few nanoseconds, and therefore significantly reduces the level of contrast degradation resulting from nanosecond fluorescence.

The OPCPA output signal beam is shaped by a programmable spatial light modulator (PSLIM) and amplified in a Nd:glass rod amplifier (RA) and disk amplifier (DA). The pulse is then compressed in the ps-GCC and can be delivered to one of three target chambers. For solid-target experiments, the STC or CTC are typically used; gas-jet and gas-cell experiments are conducted in the UDP chamber.

In the narrowband operation mode, the switchyard mirrors send the CLARA output beam directly for amplification by the RA and DA. To pump the final noncollinear optical parametric amplifier for the OPAL system, switchyard 3 is used to send the pulse
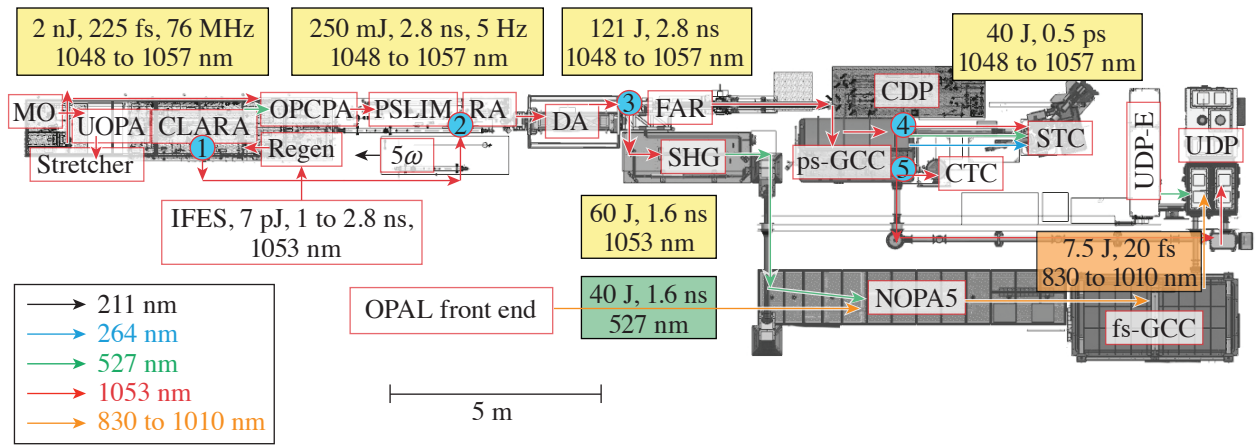
G12322JR

Figure 2

MTW laser layout. MO: master oscillator; IFES: integrated front-end system; 5ω: fifth-harmonic-generation table; FAR: Faraday isolator; CDP: compressor diagnostics package; NOPA5: the fifth nonlinear optical parametric amplifier stage; UDP-E: UDP laser; 1–5: switchyards.

to the second-harmonic-generation (SHG) table before propagating to the OPAL area. Here it is overlapped in time and space at the OPCPA crystal with the ultra-broadband seed pulse from the OPAL front end.[10] The amplified signal pulse is compressed in the femtosecond grating compressor chamber (fs-GCC) and sent to the UDP chamber.

The narrowband mode has also been used to develop technologies for the fifth-harmonic generation of joule-class, near-infrared pulses. For this, the CLARA output can be sent with or without amplification in the RA to the 5ω table, where several studies using cascades of nonlinear crystals have been performed.[16,17]

The gain nonuniformity of the RA can be precompensated by PSLIM.[18] Figure 3(a) shows the profile of the MTW output beam when the PSLIM is bypassed. Figure 3(b) shows that PSLIM can correct the mode to a flat, near-uniform beam profile. The high performance in the uniformity is the result of closed-loop operation of the PSLIM algorithm.
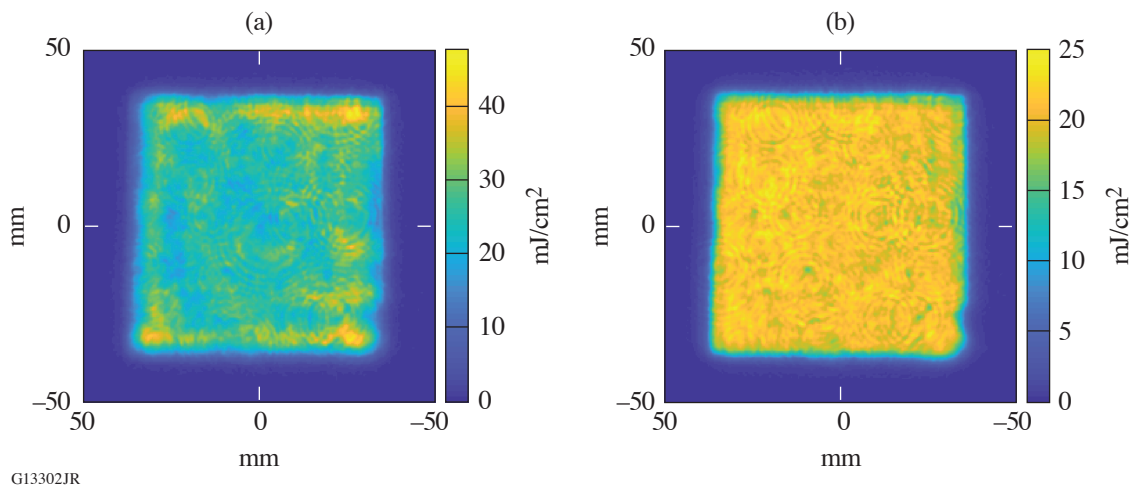
G13302JR

Figure 3

Rod amplifier beam profiles measured at the plane equivalent to the last hit of the beam on the grating in the compressor (a) without and (b) with PSLIM correction.

The on-shot MTW output energy is measured using pickoff calorimeters, which are cross-calibrated with a large-aperture calorimeter that covers a large energy range (1.5 J to 1000 J). Figure 4 demonstrates the MTW energy map at different voltages for the RA and DA. Curves show the increase in output energy versus RA input energy for different RA and DA voltages. Each point has a shot number, energy density, and peak-to-mean beam modulation.
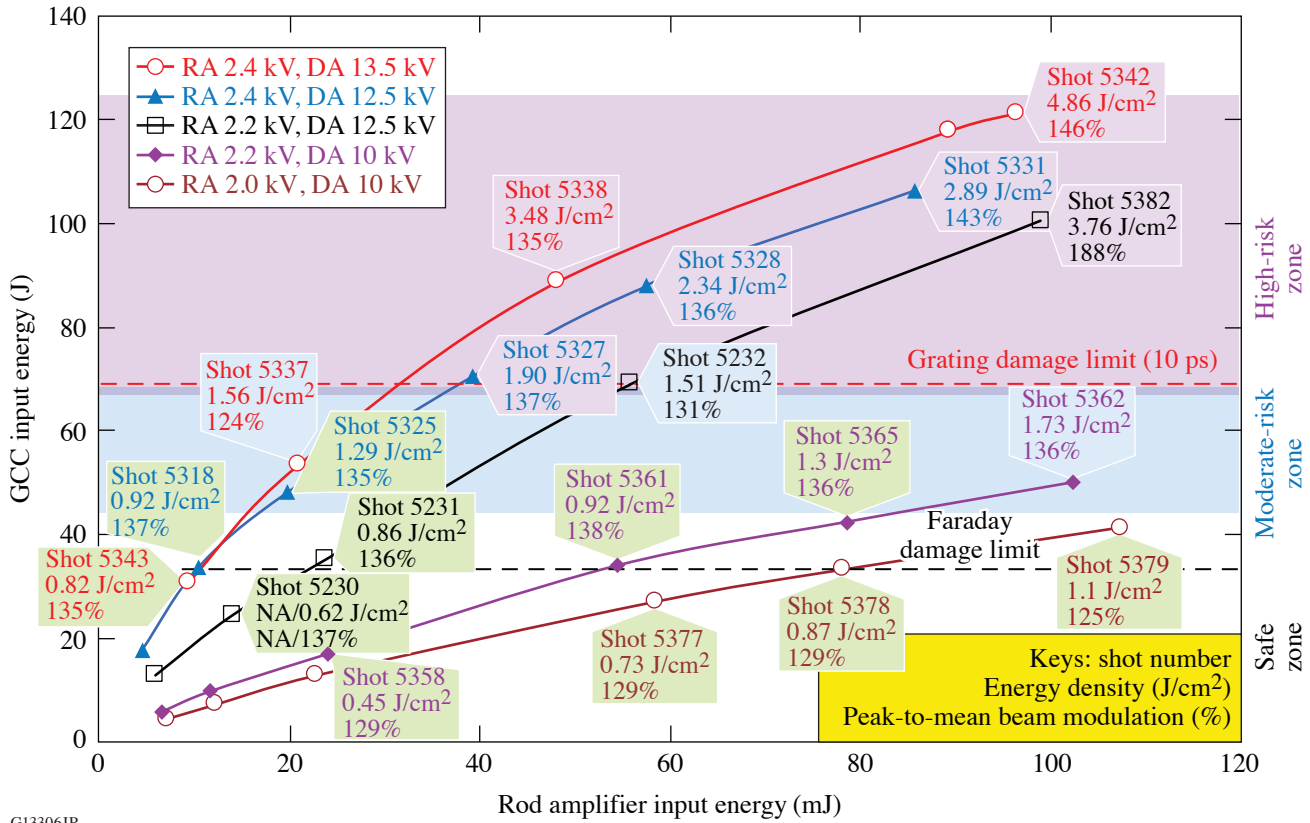

Figure 4
MTW output energy for a range of RA input energies and operating voltages for the rod and disk amplifiers. Dashed lines are damage limits imposed by the final Faraday isolator and the gratings for 10-ps pulses.

The beam propagating to the GCC and on toward the CTC and STC has two major limitations in energy; these limitations arise from the Faraday isolator and the gratings used in the compressor. The 50-J limit is set by the terbium glass damage threshold of 2 J/cm^2. The energy range below 50 J is shown in Fig. 4 as the safe zone (no shading). Because the Faraday isolator is installed before the compressor in the stretched pulse, the isolator energy limitation does not depend on the pulse duration after the compressor.

The second energy limitation is set by the damage threshold of compressor gratings, where the last hit on G1/G4 dominates. This limit does depend on the pulse duration; for example, at 10 ps, the measured damage threshold is 1.7 J/cm^2, which corresponds to the limit of output energy of 85 J. In practice, safe operation must also consider beam modulation and a safety factor of 20%, which results in a maximum energy on the final grating of approximately 70 J. The zone between 50 J and 70 J is the moderate-risk zone (blue shading), while above 70 J is the high-risk zone (purple shading). The energy on target for a 10-ps pulse is typically kept below 36 J and below 18 J for the best compression at 500 fs.

The maximum energy produced by MTW is 120 J. This is acceptable for the all-OPCPA beam path because SY3 (Fig. 2) picks the full energy beam before the last Faraday isolator.

The stretcher varies the MTW pulse duration and the sign of the chirp. A second-order scanning autocorrelator (SAC) is routinely used with the 5-Hz OPCPA beam prior to full-energy shots to measure the pulse autocorrelation width with subpicosecond precision, covering a range up to 100 ps. An autocorrelation trace of the shortest pulse is shown in Fig. 5(a) and has 497 fs at FWHM, which corresponds to a pulse duration of ~369 fs. It is shown along with a simulated autocorrelation function calculated for a transform-limited pulse based on the OPCPA's output spectrum. Both autocorrelation traces overlap well with only a 4.8% mismatch between the FWHM's.

TESSA, a time-expanded single-shot autocorrelator, is required to measure picosecond pulses when the Nd:glass amplifiers are used. It has a limit of 40 ps set by the clear aperture of the noncollinear autocorrelation crystal. Figure 5(b) shows a typical series (not taken at best compression) of single-shot autocorrelation traces, which demonstrates a highly stable operation of the MTW laser.
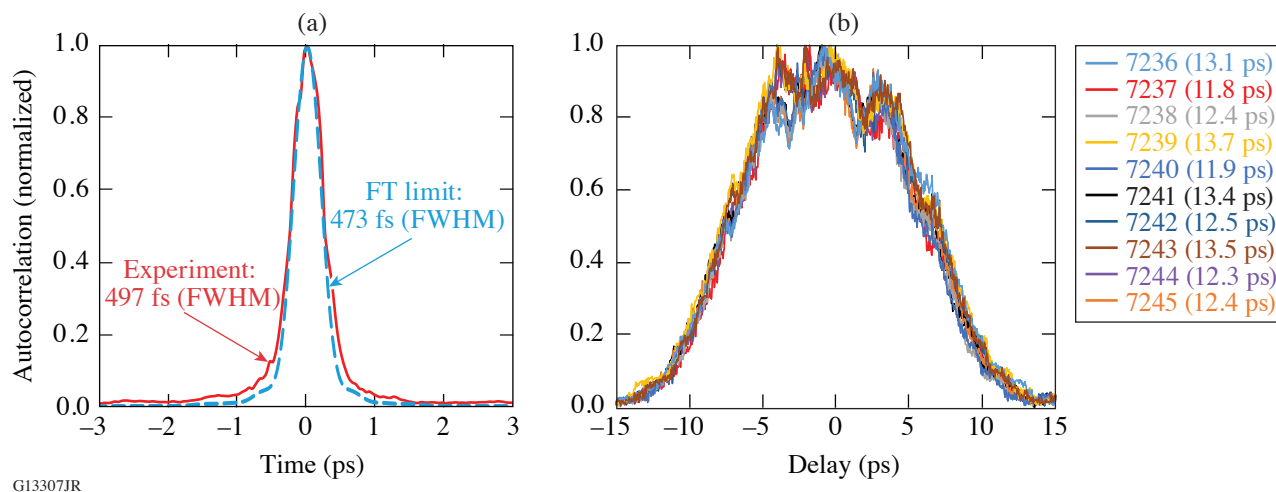

G13307JR

Figure 5

(a) The measured best-compression autocorrelation function and the simulated corresponding autocorrelation function calculated for a transform-limited pulse based on the OPCPA's output spectrum. (b) Single-shot autocorrelation traces taken by TESSA in a series of full-energy, not-the-best compression MTW shots.

To measure relatively long compressed pulses, a high-bandwidth 55-GHz photodiode and a 45-GHz oscilloscope are used. The duration of the resulting impulse response at 1053 nm is 17 ps, which overlaps with short compressed pulse diagnostics based on second-order autocorrelations. The real-time oscilloscope allows for single-shot acquisition; therefore, the diagnostic can be used on high-energy shots. The gain narrowing in the RA and the DA modifies the spectrum of the MTW beam. The changes on the spectrum and, therefore, on the recompressed pulse duration depend on the voltage from each amplifier and OPCPA output energy. Figure 6 shows pulse durations after the picosecond compressor measured with different diagnostics, depending on the stretcher translation stage position referenced to its position for best compression.

The nonlinear cross-correlator provides MTW temporal contrast information with high temporal resolution over an ~200-ps temporal window [Fig. 7(a)], while the high-contrast photodiode provides single-shot contrast information over a much larger temporal window with resolution limited by the bandwidth of the photodetector and oscilloscope, approximately 200 ps [Figs. 7(b) and 7(c)].

The focal spot of the MTW output beam is measured at the focus of the $f/2$ off-axis parabola in the center of the STC using a 12-bit camera and a 10× objective microscope. An attenuation of 10^6 is achieved using two 0.1% leaky wedged mirrors installed in an "antiparallel" configuration inside the GCC. Additional attenuation is provided using neutral-density filters. A typical focal spot is shown in Fig. 8(a) and has a slightly elliptical shape with major and minor axes widths of 6 μm and 5 μm, respectively; 85% of the energy is contained in a circle with a 5-μm radius [Fig. 8(b)].
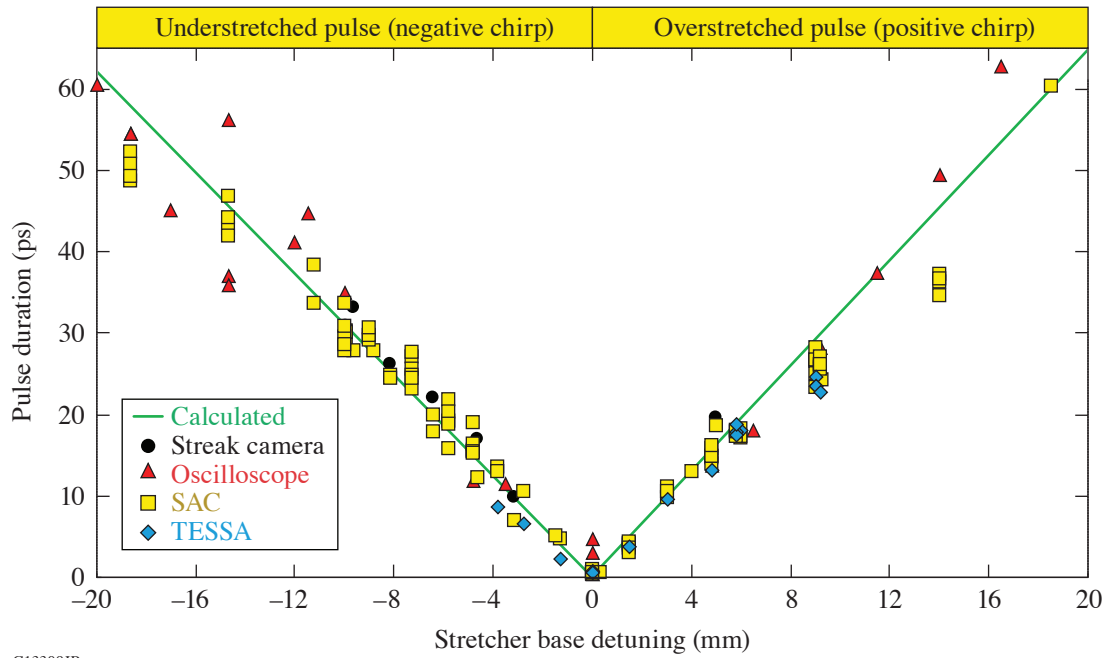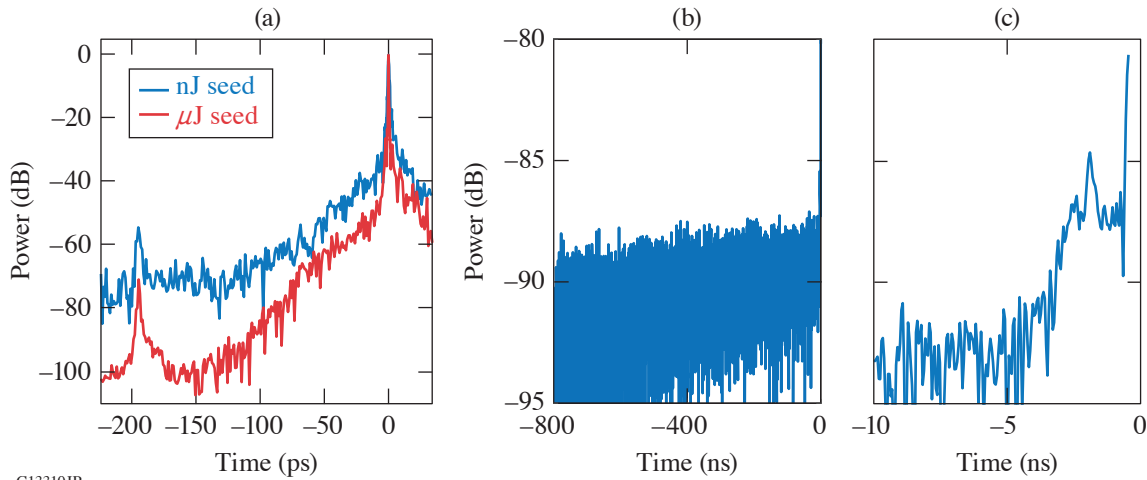
Figure 6
Compressed pulse duration adjustment by the stretcher.

G13309JR

G13310JR

Figure 7
Temporal contrast of the compressed MTW pulse measured with (a) the nonlinear cross-correlator and [(b),(c)] with a photodiode and oscilloscope. In (a), the temporal contrast is shown before and after UOPA deployment.

The MTW wavefront is measured by a wavefront sensor. This measurement requires careful calibration of non-common-path wavefront aberrations in the diagnostic path and a determination of the single-pass contribution through the compressor. A typical MTW wavefront for a single pass through the GCC is shown in Fig. 9 and has a peak-to-valley (p–v) variation of 0.15 λ over 98% of the MTW beam.

The main applications of the MTW laser include high-energy-density science,[19,20] x-ray spectrometers,[21] neutron diagnostic development,[22] and "flying focus"—a concept where the combination of temporal chirp and longitudinal chromatic aberration
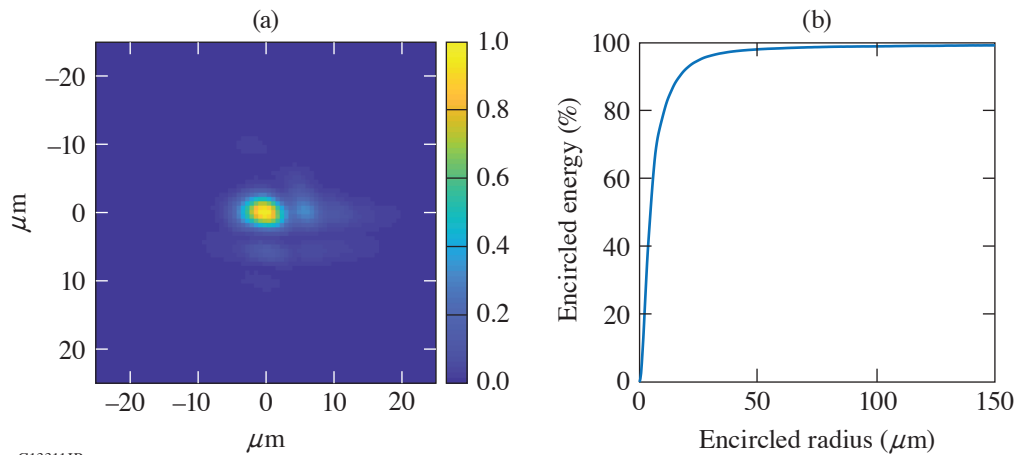
(a)

(b)

G13311JR

Figure 8
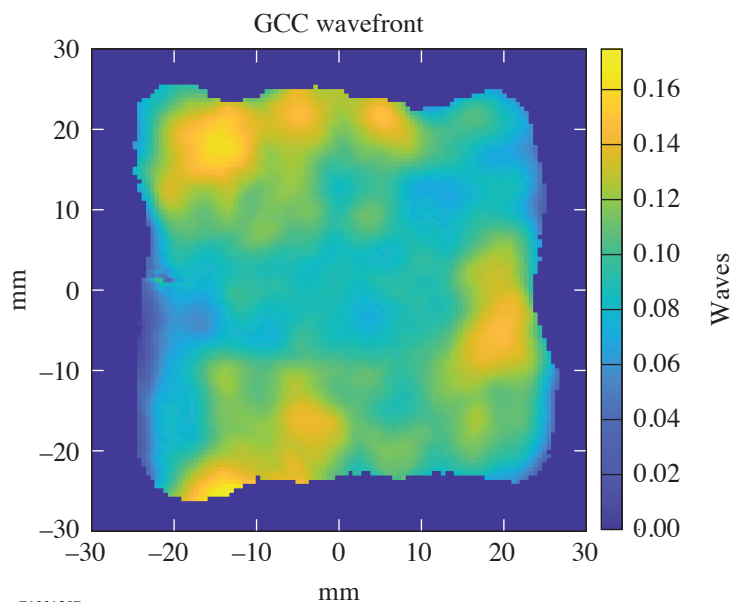Focal spot of an MTW beam.

GCC wavefront

G13312JR

Figure 9
MTW output wavefront, with a 0.15 λ (p–v) modulation.

provides unprecedented spatiotemporal control over the velocity of a high-intensity focal spot over distances far exceeding the Rayleigh length.[23] Efforts are underway to use MTW for parametric amplification; using stimulated Raman scattering in a plasma which could be an enabling technology in the generation of ultrahigh-power laser pulses.[24]

Many experiments on MTW require wavelengths different from the 1053-nm fundamental. For example, picosecond time-resolved measurements of dense plasma line shifts[25] require the second harmonic. Timing calibration of x-ray streak cameras requires short subpicosecond pulses in the deep-UV region. Fifth-harmonic generation is necessary for many plasma diagnostics.[26,27] To satisfy these requirements and to increase the temporal contrast of compressed pulses,[28] the MTW output beam can be converted into the second, fourth, and fifth harmonics.

MTW was built based on the most-recent laser technologies and continues to develop novel ideas in laser science and engineering while also providing a flexible platform for development of frontier laser and plasma diagnostics.

1. S. Gales *et al.*, Rep. Prog. Phys. **81**, 094301 (2018).

2. A. L. Kritcher *et al.*, Nature **584**, 51 (2020).

3. G. H. Miller, E. I. Moses, and C. R. Wuest, Opt. Eng. **43**, 2841 (2004).

4. J. H. Kelly *et al.*, J. Phys. IV France **133**, 75 (2006).

5. J. Ebrardt and J. M. Chaput, J. Phys.: Conf. Ser. **244**, 032017 (2010).

6. C. N. Danson *et al.*, Nucl. Fusion **44**, S239 (2004).

7. G. Xu *et al.*, Rev. Laser Eng. **36**, 1172 (2008).

8. V. V. Lozhkarev *et al.*, Laser Phys. Lett. **4**, 421 (2007).

9. C. N. Danson *et al.*, High Power Laser Sci. Eng. **7**, e54 (2019).

10. J. Bromage *et al.*, High Power Laser Sci. Eng. **7**, e4 (2019).

11. J. R. Marciante and J. D. Zuegel, Appl. Opt. **45**, 6798 (2006).

12. A. V. Okishev *et al.*, in Advanced Solid-State Lasers, edited by M. E. Fermann and L. R. Marshall, OSA TOPS Vol. 68 (Optical Society of America, Washington, DC, 2002), pp. 418–422.

13. V. Bagnoud *et al.*, Appl. Opt. **44**, 282 (2005).

14. V. Bagnoud *et al.*, Opt. Lett. **30**, 1843 (2005).

15. C. Dorrer, A. V. Okishev, and J. D. Zuegel, Opt. Lett. **32**, 2143 (2007).

16. I. A. Begishev *et al.*, Opt. Lett. **43**, 2462 (2018).

17. I. A. Begishev *et al.*, Opt. Express **29**, 1879 (2021).

18. S.-W. Bahk, I. A. Begishev, and J. D. Zuegel, Opt. Commun. **333**, 45 (2014).

19. P. M. Nilson *et al.*, J. Phys. B: At. Mol. Opt. Phys. **48**, 224001 (2015).

20. M. Storm *et al.*, Rev. Sci. Instrum. **79**, 10F503 (2008).

21. C. R. Stillman *et al.*, Rev. Sci. Instrum. **87**, 11E312 (2016).

22. C. Stoeckl *et al.*, Rev. Sci. Instrum. **87**, 053501 (2016).

23. D. H. Froula *et al.*, Nat. Photonics **12**, 262 (2018).

24. D. Turnbull *et al.*, Plasma Phys. Control. Fusion **61**, 014022 (2019).

25. C. R. Stillman *et al.*, Phys. Rev. E. **95**, 063204 (2017).

26. J. S. Ross *et al.*, Rev. Sci. Instrum. **81**, 10D523 (2010).

27. V. V. Ivanov, A. A. Anderson, and I. A. Begishev, Appl. Opt. **55**, 498 (2016).

28. D. Hillier *et al.*, Appl. Opt. **52**, 4258 (2013).